# Dynamics of Polymers in Organosilicate Nanocomposites

**Xuesong Hu,[†] Wenhua Zhang,[†] Mayu Si,[†] Michael Gelfer,[‡] Benjamin Hsiao,[‡] Miriam Rafailovich,*[,†] Jonathan Sokolov,[†] Vladimir Zaitsev,[§] and Steven Schwarz[§]**

*Department of Materials Science & Engineering, State University of New York, Stony Brook, New York 11794-2275, Department of Chemistry, State University of New York, Stony Brook, New York 11794, and Department of Physics, Queens College of City University of New York, Flushing, New York 11367*

*Received June 17, 2002*

ABSTRACT: Dynamic secondary ion mass spectrometry (DSIMS) measurements were performed to measure the effects of functionlized organosilicate clay (Cloisite 6A) on the tracer diffusion coefficient, *D*, in polystyrene (PS) and poly(methyl methacrylate) (PMMA) matrices. The results indicate that *D* is unaffected by the addition of 5% (by volume) of PS and is reduced by a factor of 3 with the addition of the same volume fraction in a PMMA matrix. The same ratio was also obtained for the extrapolated zero shear rate viscosity of PS and PMMA melt-mixed composites with the same volume fraction of clay. DSIMS was also used to measure the mobility of the clay platelets, which was found to be much lower than the polymer chains in both matrices. Examination of the sample morphology with scanning force and transmission electron microscopy indicated that in contrast to melt mixing, spin casting produced a large degree of exfoliation in both PS and PMMA matrices. Hence the difference in the dynamics in the presence of clay was ascribed to preferential interactions between the PMMA polymer and the platelet surface, rather than the extent of exfoliation.

## Introduction

Layered silicates are increasingly used to enhance materials properties of polymer,[1−5] such as gas impermeability,[2,3] stiffness/impact balance,[2] and flame retardance.[2,3] To incorporate these polymers into actual components, it is also important to understand the effect of the clays on processing parameters such as adhesion, rheology, and viscosity. The diffusion coefficient of polymer chains in the melt is an important factor in determining the effect of clays on these physical processes. Here we concentrate on studying the tracer diffusion coefficients, *D*, of polystyrene (PS) and poly(methyl methacrylate) (PMMA) chains in polymer−clay nanocomposite thin film systems, using dynamic secondary ion mass spectrometry (DSIMS). This work is somewhat different from previous studies by other groups who concentrated on the dynamics of polymer chains intercalated into layered silicates structures.[6−10] Here we show that when functionlized montmorillonite clays are spun cast together with polymers from solution, a large degree of exfoliation and orientation of the platelets occurs. We therefore focus here on the effect on polymer mobility by asymmetric obstacles with differential interactions between the clay surfaces and the matrix polymer chains.

## Experimental Section

Cloisite 6A (Southern Clay Products), a hydrogenated tallow functionalized montmorillonite clay, and monodisperse ($M_w/M_n$<1.04) polystyrene (PS) and poly(methyl methacrylate) (PMMA) (Polymer Laboratories), as well as their deuterated analogues, were used in these experiments. The specifications are listed in Table 1. Bilayer substrates were prepared as follows: initially a layer of hydrogenated polymer was spun cast from toluene solution directly onto HF stripped Si wafers. The thickness of this layer, typically 100 nm, was measured with ellipsometry. Another layer containing 20% deuterated polymer and 80% hydrogenated polymer was spun cast onto a glass slide and floated from DI water onto the completely hydrogenated layers. Then 5 vol % of silicate was added directly to the polymer solution and spun cast together with the films. Clay was added to the upper or lower layer or both. Control samples without clay were also made for direct comparison. A schematic of the different sample geometries is shown in Figure 1. The PS and PMMA bilayer samples were then annealed at 137 and 170 °C, respectively, in an oil-trapped vacuum of $10^{-3}$ Torr for times ranging from 1 to 24 h.

**Table 1. Characteristics of Polymers Used in This Study**

| | $M_w$ | $M_w/M_n$ |
|---|---|---|
| PS | 94 000 | 1.04 |
| dPS | 96 000 | 1.02 |
| PMMA | 55 900 | 1.03 |
| dPMMA | 65 000 | 1.03 |

To determine whether preferential adsorption of one of the polymer occurred we devised a method of forming a planar macroscopic clay surface. Shin et al.[11] have shown that when Cloisite 6A is spread from chloroform solution at the air−water interface with a surface pressure of 25 mN/m, a uniform monolayer film of close packed platelets is formed. We followed his spreading protocol and lifted the film onto a Si wafer. The uniformity and thickness were checked by examining the surface with scanning probe microscopy (SPM). A polymer blend film composed of 0.80 PS and 0.20 PMMA was spun cast onto a glass slide and lifted from the water surface onto the clay-coated Si wafer. The sample was then annealed for 1 h at 170 °C. This time was chosen to be sufficient to allow segregation, but too short to allow dewetting.

After annealing, all samples were covered with a 50 nm thick sacrificial layer, and the concentration profiles were studied by dynamic secondary ion mass spectrometry (DSIMS) using either an Atomika 3000−30 SIMS or a ION TOF IV spectrometer.

In each case, the intensity of emitted ions ($H^-$, $D^-$, $C^-$, $O^-$, $Si^-$, etc.) was measured as a function of sputtering time and converted to concentration vs time profiles using the known film thickness. In the Atomika instruments, (DSIMS) was

[†] Department of Materials Science & Engineering, State University of New York, Stony Brook.
[‡] Department of Chemistry, State University of New York, Stony Brook.
[§] Queens College of City University of New York.

10.1021/ma020937f CCC: $25.00 
Published on Web 01/11/2003

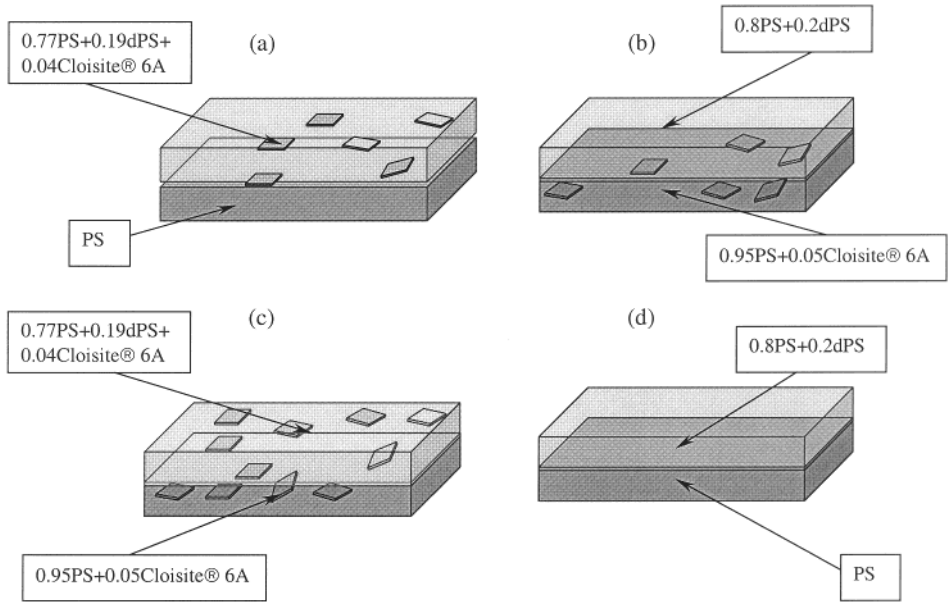


**Figure 1.** Sample geometry for the tracer diffusion measurements. In all cases the lower film was spun cast onto Si wafer and the upper layer was floated. Samples a−c contain Cloisite 6A clay while sample d is the control sample.

performed by bombarding the sample with a 2.0 keV Ar ion beam at 45° incidence. For the TOF−SIMS, a 25 keV beam of $^{69}Ga^+$ ions, with a pulse width of 100−200 ns incident at 45° off normal incidence was used for imaging. A 3 keV, 40 nA beam of $^{133}Cs^+$ ions, aimed at 45° off normal incidence rastered over a 200 × 200 $\mu m^2$ crater size, was used for sputtering. A 20 eV, 5 $\mu$A electron beam was used for charge compensation. The resolution of DSIMS was less than 8 nm for the Atomika and 4 nm for the TOF−SIMS instruments. The mass sensitivity for heavier fragments is superior in the TOF−SIMS, and hence, it was used to image the Si ion concentration, which was assumed to be proportional to the clay concentration in the sample. We compared the sputtering rate of the samples in the four geometries and found no noticeable difference in the sputtering rates between samples with and without clay, even when the layers with and without clay were in the same sample (geometries a and b).

The distribution of clay in the samples was imaged with a DI3000 scanning probe microscope using a silicon nitrite tip, in the contact mode. Some samples were removed from the silicon wafers, floated onto thick polyamide substrates, and sectioned using a Reichert microtone at room temperature. The samples were then imaged with a JEOL TEM 1200EX scanning transmission electron microscope. Electron contrast was possible without stain, since clay is much more electron dense than either the PS or PMMA polymer matrices.

For the bulk rheological measurements polydisperse PS (Aldrich Chemical, $M_w = 280$K) and PMMA (Aldrich Chemical, $M_w = 120$K) were used. The nanocomposites were prepared by mixing the respective homopolymer with 5 vol % of Cloisite 6A in a Brabender twin-screw melt-mixer at 170 °C with a mixing speed of 100 rpm for 10 min. The rheological samples were prepared by placing the mixed samples in stainless steel 25 mm diameter, 2 mm thick, cylindrical molds and pressed for a total of 10 min at 170 °C. To maintain flat surfaces, the steel molds were covered with heat resistant Kapton films. Rheological measurements were performed using a Rheometrics Scientific RMS 650 strain-controlled rheometer. Steady shear experiments were performed using 25 mm parallel plates. The data were acquired during the shear rate sweep ($0.05 < \gamma' < 20\ s^{-1}$) at each temperature. To avoid degradation of the sample, all rheological experiments were performed under nitrogen gas flow.

## Results and Discussion

**Distribution of the Clay Platelets in the Films.** SPM images of spun-cast PS and PMMA films containing 5 vol % of clay are shown in Figure 2. From the figure, we see that the topographical images are relatively smooth with an rms roughness of approximately 2.5 nm with no distinct features. On the other hand, large irregularly shaped regions of lower friction than the surrounding areas are seen in the lateral force images. These regions are interpreted as being due to the clay platelets, which are harder than the PS matrix and resist penetration by the SPM tip. Hence the reduced contact area induces lower friction. Comparing with the topographical image, where the platelets are not visible, we conclude that the platelets are probably

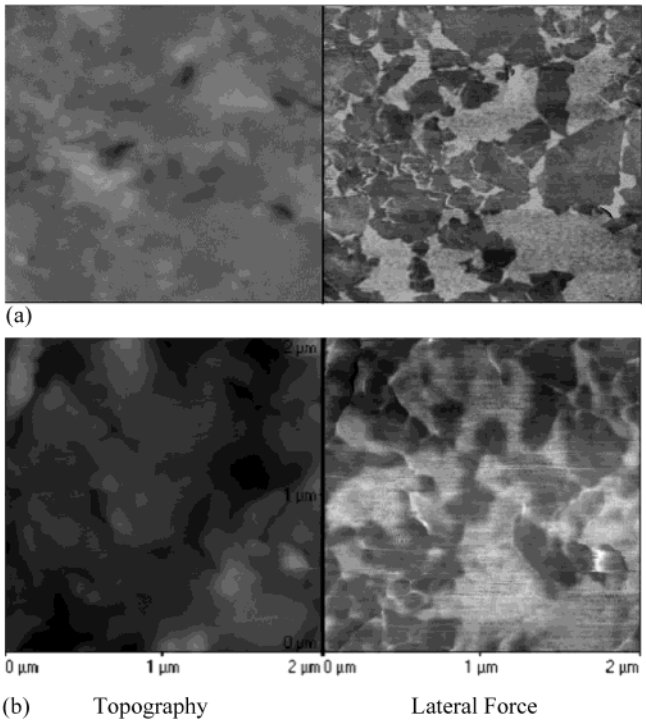


**Figure 2.** Topography and lateral force images of spun cast PS (a) and PMMA (b) films, 100 nm thick, containing 5% Cloisite 6A clay. The RMS roughness in each case was approximately 2 nm.

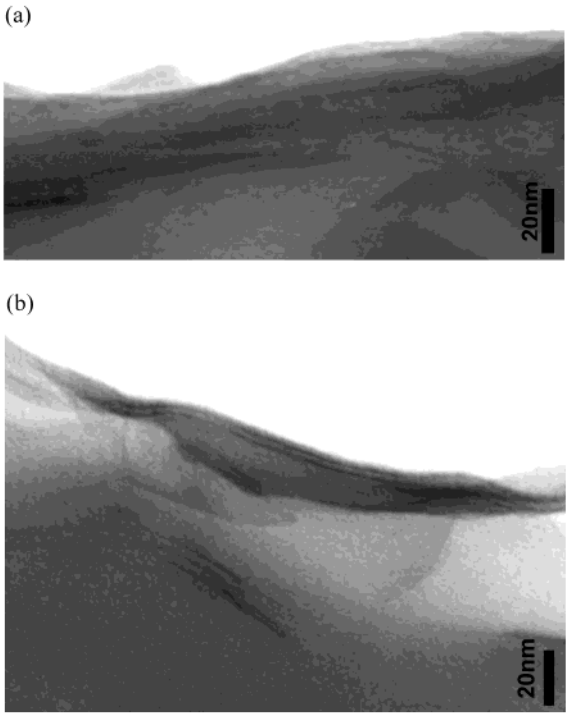


**Figure 3.** TEM micrographs of microtomed PS (a) and PMMA (b) films containing 5 vol % Cloisite 6A spun cast onto polyamide surfaces.

covered by a thin layer of polymer. The lateral dimension of the platelets, on the order of several hundred nanometers, is consistent with previous measurements[11] on clay monolayers, deposited on silicon wafers by the Langmuir−Blodgett method. From the lateral force image we can clearly see that the aerial density of the clay is, approximately 75%, which is much larger than the volumetric composition of *5%*. A rough estimate indicates that the thickness of the clay tactoids would be approximately 5−6 nm, or a large degree of exfoliation and orientation parallel to the film surface is present. These observations are confirmed by the TEM micrographs shown in Figure 3 of microtomed PS and PMMA films spun cast onto polyamide substrates with 5% clay. Here we can see that while some of the platelets contain single layers, approximately 70% are composed of two layers with a total thickness of 4−6 nm, in agreement with the SPM figures, while very few tactoids are composed of three or more layers. The fact that the platelets are also highly oriented is not surprising since the aerial dimensions of the platelets is approximately on the order of the film thickness. The platelets are therefore confined to lie parallel to the surface if they are to minimize deformation.

In melt-processed samples it is difficult to partially exfoliate clay in PMMA and nearly impossible in PS matrices.[8] In thin films, on the other hand, the solvent penetrates easily into the clay galleries. The shear imposed on the solution during spin casting is much larger than what can be applied mechanically in a melt processor. Hence, when spun cast from solution, it is easy to obtain a high degree of exfoliation in almost any polymer regardless of the polymer/clay interaction.

**Dynamic Secondary Ion Mass Spectrometry (DSIMS).** To determine the effect of clay on the chain dynamics, the diffusion in four types of bilayer samples, shown in Figure 1, was studied. The samples were all annealed under identical conditions and then the concentration profiles were measured using dynamic SIMS. The raw data from TOF−SIMS, plotted as counts vs sputtering time, for a bilayer film of the geometry shown in the inset, before and after annealing at 137 °C for 6 h is shown in Figure 4, parts a and b, respectively. From the figures, we see that the carbon trace is a good indicator of the distribution of the polymer layer, which does not change with annealing. The counts in the Si trace are seen to rise as the carbon trace decreases marking the interface with the substrate. The Si counts within the upper layer of the sample indicate the presence of clay. Similarly, a large oxygen peak, corresponding to surface oxides, marks the polymer silicon interface. Oxygen counts also appear within the upper deuterated layer. This profile mirrors the Si counts and is assumed to originate from the di-tallow surfactant coating the clay platelets, which are present in the upper layer only. Minimal oxygen is present in the lower PS layer, as expected. In the unannealed sample, the deuterium trace forms a sharp interface with the lower hydrogenated layer. Surface segregation is seen in both the Si and oxygen traces associated with clay. After annealing, the deuterium trace broadens, indicating diffusion into the hydrogenated lower layers. The oxygen and Si traces also broaden, but to a lesser extent,

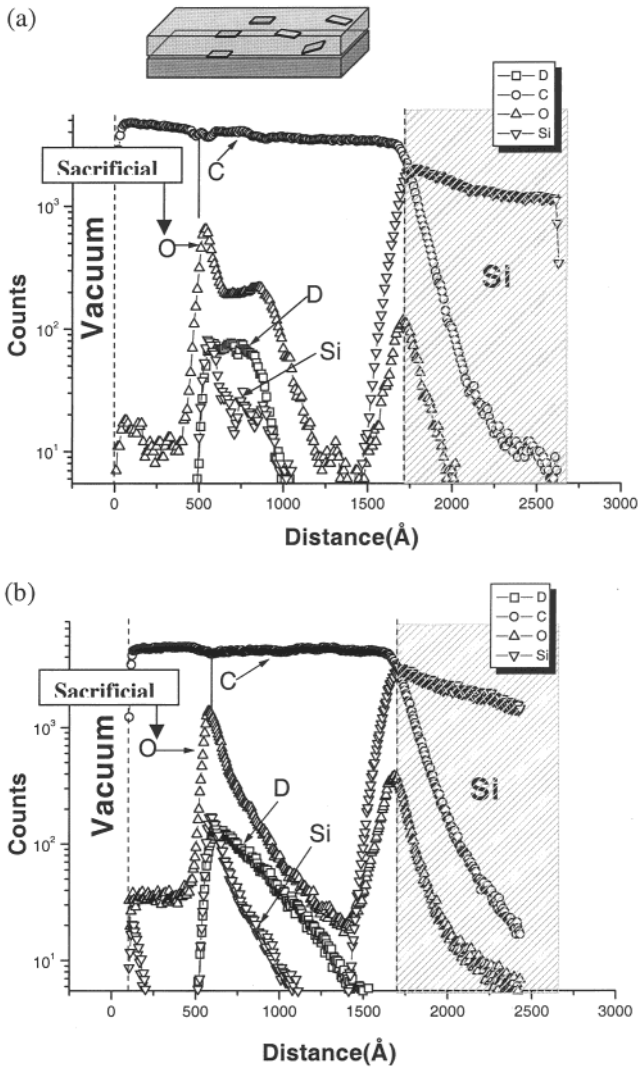


**Figure 4.** TOF−SIMS spectra from a bilayer sample corresponding to the geometry shown in Figure 1a (a) prior to annealing and (b) after annealing at 137 °C for 6 h.

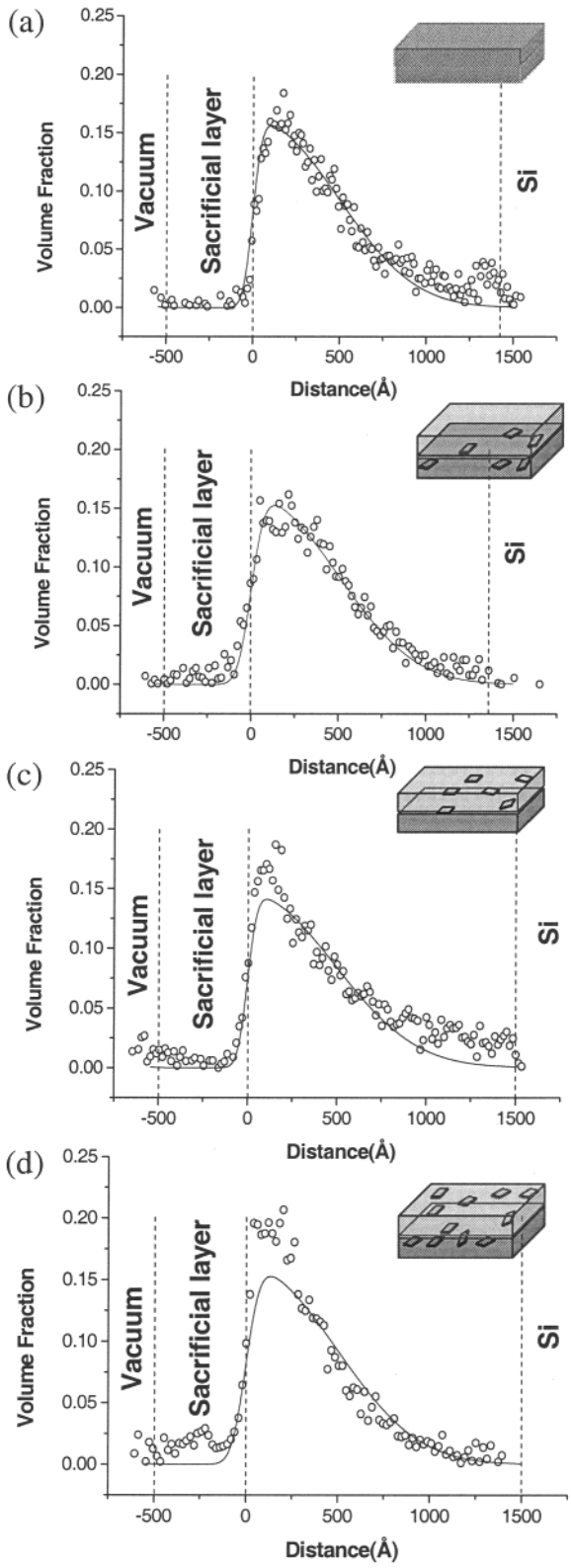


**Figure 5.** DSIMS profiles of the deuterium distribution in dPS/PS bilayer samples with 5% volume fraction of Cloisite 6A annealed at 137 °C for 6 h. The cartoons in the inset correspond to the different geometries. The solid lines are fits to eq 1.

indicating that the clay platelets are much less mobile than the polymer chains.

The concentration profiles of the dPS, obtained from the intensity of the sputtered deuterium ions, are plotted as a function of distance from the sample surface for each sample geometry in Figure 5. The solid lines are fits to the Fickian equation for diffusion from a semi-infinite sample:[12,13]

$$\phi(x) = 0.5\ \mathrm{erf}[(h - x)/\sqrt{4Dt}] + 0.5\ \mathrm{erf}[(h + x)/\sqrt{4Dt}] \quad (1)$$

where $D$ is the constant tracer diffusion coefficient of the polymer chains, $x$ is the distance from the interface, and $h$ is the sample thickness. The diffusion coefficients that provide the best fit to the various spectra are tabulated in Table 2 where we can see that they vary by no more than 20% for the different geometries. Hence we conclude that even though the clay platelets are widely dispersed within the sample, they do not affect the mobility of the PS chains.

**Table 2. Summary of the Tracer Diffusion Coefficients $D$ ($cm^2/s$) in dPS/PS and dPMMA/PMMA Bilayers Obtained from for Samples in the Geometries Shown in Figure 1**

| | | diffusion coeff $D$ ($\times 10^{-16}$ $cm^2/s$) | | | |
|---|---|---|---|---|---|
| sample | annealing time/temp | geometry 1(d) | geometry 1(b) | geometry 1(a) | geometry 1(c) |
| PS | 6 h/137 °C | 3.0(3) | 3.0(3) | 3.5(3) | 3.0(3) |
| PMMA | 8.5 h/170 °C | 4.0(4) | 1.4(1) | 1.2(1) | 0.50(5) |

To determine the mobility of the clay platelets, the Si distribution within the samples was studied using TOF−SIMS. The data are shown in Figure 6 for the three geometries shown in the inset. From Figure 6a, we can see that when clay is present in the layer adjacent to the vacuum surface, preferential segregation of platelets to the near surface region occurs immediately after spinning. Further annealing of the samples up to 12 h does not change the distribution of the clay within the sample. In Figure 6b, we show the profiles of samples where clay was present in the layer adjacent to the Si substrate. Since this layer was first prepared by spin casting the lower layer from solution, we find some segregation in the unannealed samples to the original free surface of the substrate. After annealing, some of the clay is seen to segregate to the silicon interface. Most of the motion occurs after 1 h of annealing, and no further motion occurs even after 12 h of annealing. This set of data shows that the clay platelets are mobile within the sample, but appear to reach their equilibrium distribution fairly quickly.

In Figure 6c, we show the clay distribution when platelets are present in both top and bottom layers. The profiles appear to be composites of those where the clay was present in either one of the layers. Even though segregation of clay occurs immediately after casting to both vacuum and silicon interfaces, a significant volume fraction, $\phi = 0.04$, remains at the interface between the two layers and in the bulk of the film. As in the previous samples, annealing does not seem to alter the initial distribution of the clay platelets.

In Figure 7, we plot the clay distribution in a bilayer sample containing PMMA in the bottom layer. From the figure, we find that the distribution is similar to that measured for the PS matrix. Clay segregates to the substrate, immediately after spinning, and the profile is unaltered upon further annealing.

The concentration of clay platelets in the films can also be estimated from the TEM micrographs, shown in Figure 3. The value obtained 5.5 and 4.5 for PS and PMMA are in good agreement with the volume fraction within the film obtained with TOF−SIMS. The surface-

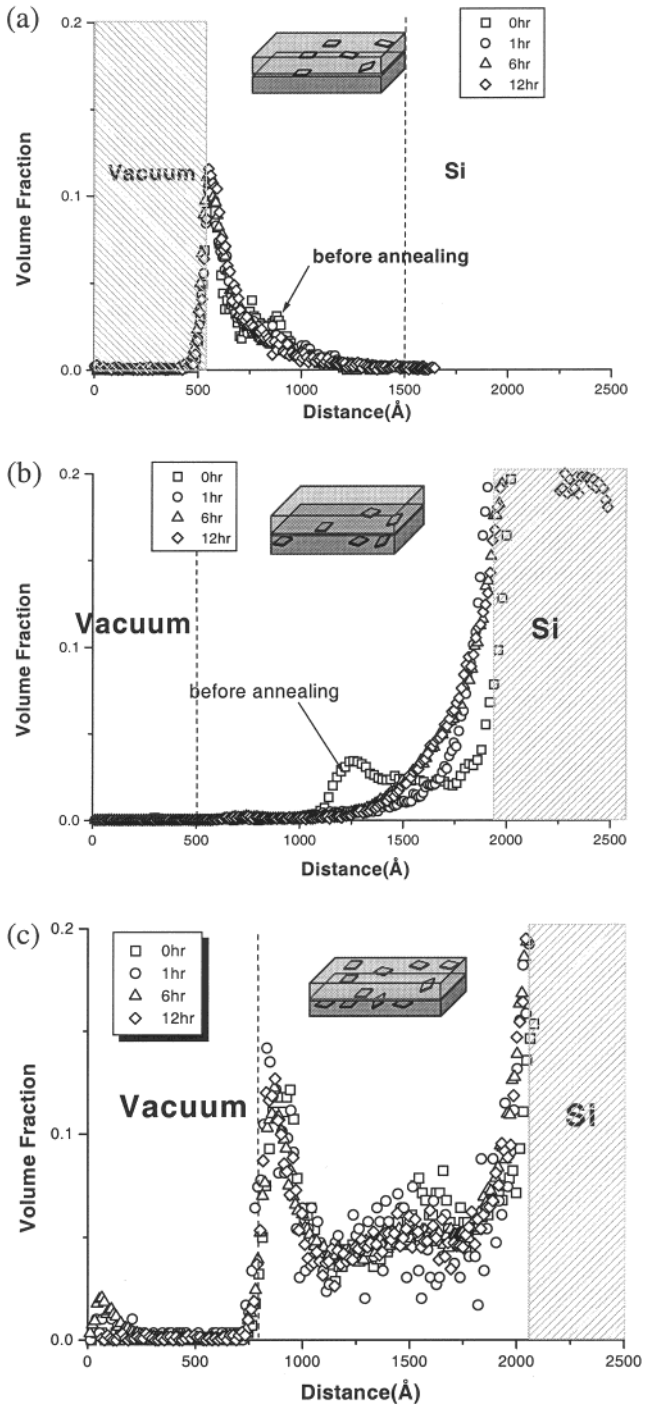


**Figure 6.** Volume fraction of Si plotted vs distance from the vacuum interface for dPS/PS bilayer samples in the geometries shown in the inset. The concentration of Si in the sample is assumed to be proportional to the clay concentration. The profiles were measured before and after annealing for each sample as indicated in the figure.

enriched layer observed with SIMS is somewhat difficult to observe with TEM since it appears to be distorted by the microtoming process. Despite the large degree of exfoliation the distribution of clay platelets within either films is too small to produce an impenetrable barrier to chain diffusion within either sample.

In Figure 8, we plot the dynamic SIMS profiles of the deuterium distribution in dPMMA/PMMA bilayer samples with 5% fraction of Cloisite 6A. From the figure we clearly see that the introduction of clay in any of the layers significantly reduces the interfacial width as

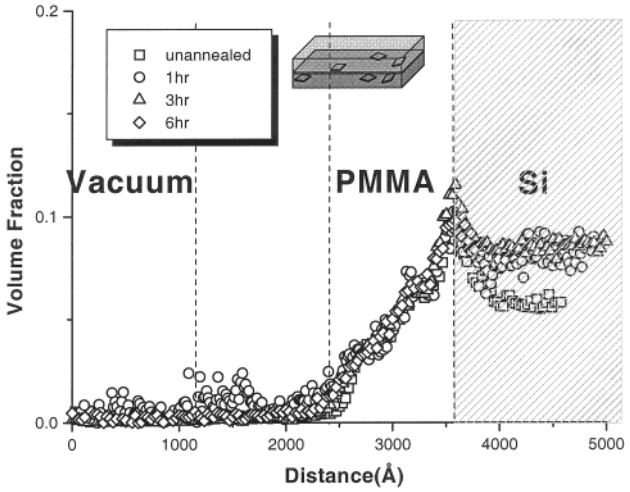


**Figure 7.** Clay distribution in a dPMMA/PMMA sample with 5 vol % of Cloisite 6A in the geometry shown in the inset. The sample was annealed for various times as shown.

compared to the unfilled bilayer sample. The solid lines are fits to eq 1 and the tracer diffusion coefficients obtained for each geometry are tabulated in Table 2. From the table we find that adding clay in only one layer, top or bottom, reduced the tracer diffusion coefficient by roughly $^1/_3$, from $D = 4 \times 10^{-16}$ cm$^2$/s to $D = 1.4 \times 10^{-16}$ cm$^2$/s. Introducing clay in both layers decreased $D$ by another factor of $(3-0.5) \times 10^{-16}$ cm$^2$/s.

Since we know from Figure 7 that the clay does not diffuse between layers, reduction in the diffusion coefficient seems to be proportional to the volume traversed by a polymer chain where clay is present. Placing clay in both layers, yields the intrinsic tracer diffusion coefficient in a matrix with a uniform volume fraction of clay. The diffusion observed between layers with and without clay, represents an average between the tracer diffusion coefficient in the filled and unfilled homopolymer matrices. The amount of diffusion that occurs will be determined simply by the time spent in each domain. Since, as shown in Figure 7, the dispersion of the clay in the spun cast samples does not differ greatly between the PS and PMMA matrixes, the difference in the effect on the chain mobility must be due to a difference in the interaction energies between the two matrices and the clay surfaces.

To determine whether preferential adsorption of one of the polymers occurred, we studied the distribution of dPMMA in a PS/dPMMA blend film deposited onto a clay-coated Si wafer. The DSIMS spectra are shown in Figure 9 after annealing at 170 °C for 1 h. From the figure, it is clear that preferential segregation of the dPMMA to the substrate interface occurs. This favorable attraction is consistent with the slower dynamics observed in the PMMA matrix.

**Steady Shear Rheological Behavior.** The dependence of the viscosity ($\eta$) on the shear rate for PS and PMMA and their corresponding nanocomposites with 5% Cloisite 6A is shown in Figure 10. In each case, the data were fit to a modified Cross model[14,15] given by

$$\eta = \frac{\eta_0}{1 + \left(\frac{\eta_0}{\tau^*}\gamma'\right)^{1-n}} \qquad (2)$$

Here $\eta_0$ represents the apparent zero shear rate viscos-

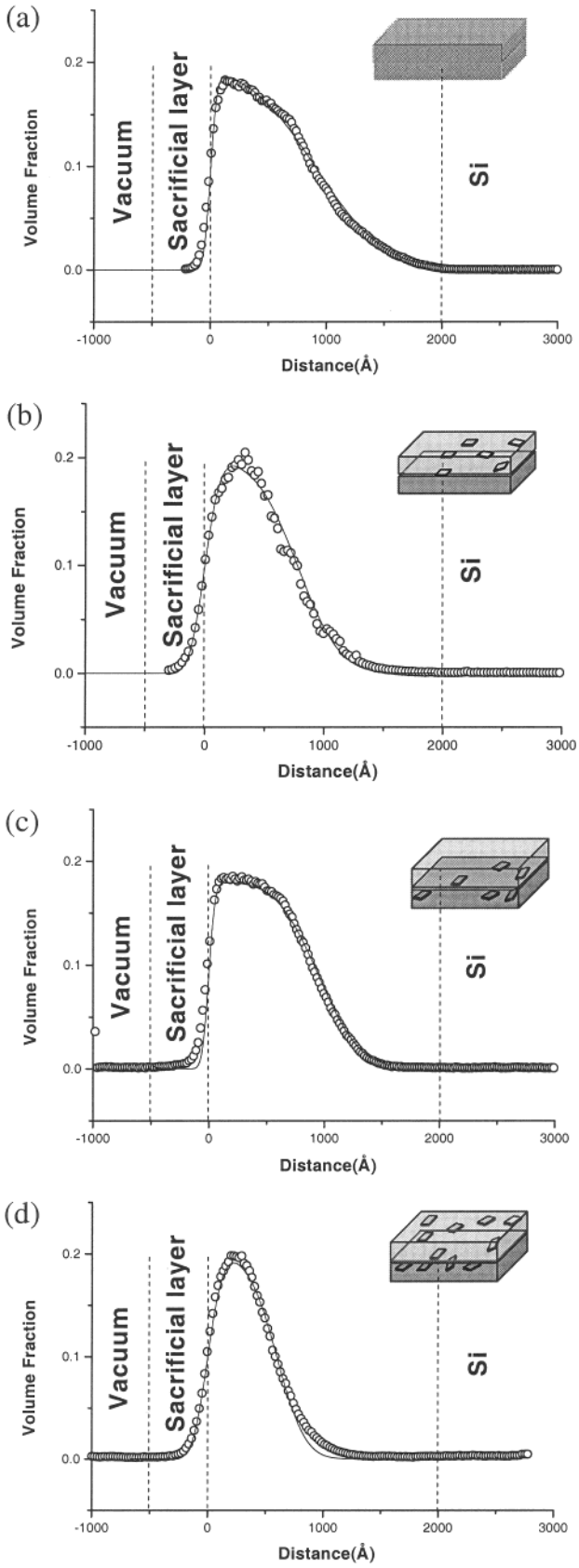


**Figure 8.** DSIMS profiles of the deuterium distribution in dPMMA/PMMA bilayer samples with 5% volume fraction of Cloisite 6A annealed at 170 °C for 8.5 h. The cartoons in the inset correspond to the different geometries. The solid lines are fits to eq 1.

ity, $\tau^*$ is the critical shear stress characterizing the transition shear stress from the Newtonian range to the pseudo-plastic region, and $n$ represents the shear rate sensitivity.

It should be mentioned that filled polymer systems often reveal Bingham-type rheological behavior, which implies that the viscosity diverges at zero shear rates.[15] Thus, for the nanocomposites the $\eta_0$ parameter cannot be measured directly, but an apparent value can be determined by extrapolating the $\eta(\gamma^{\bullet})$ curves (eq 2) to

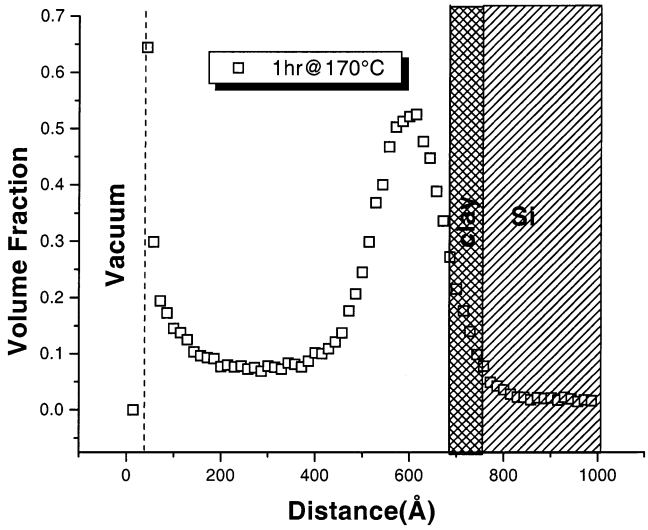


**Figure 9.** DSIMS concentration profile of a blend composed of 0.80 hPS and 0.20 dPMMA spun cast on glass and floated onto a Si wafer coated with a monolayer of Cloisite 6A applied by the Langmuir−Blodgett technique. The profiles for the sample as floated and after annealing at 170 °C for 1 h are shown.

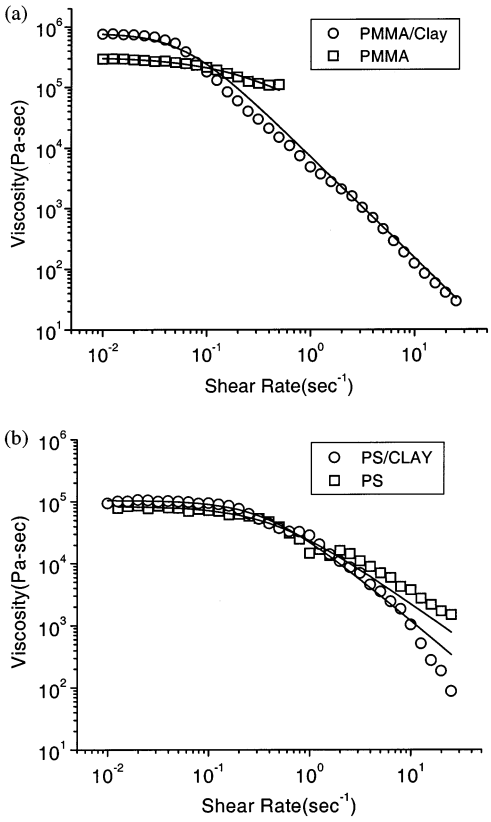


**Figure 10.** Viscosity ($\eta$) as a function of the shear rate for the pure homopolymer and 5 vol % Cloisite 6A nanocomposite produced by melt mixing with (a) PS and (b) PMMA. The solid lines in each case are fits to eq 2.

**Table 3. Zero-Shear Rate Viscosity Measurements Performed at 170 °C under Nitrogen Flow, for PS and PMMA with or without 5% Clay**

| sample (170 °C) | extrapolated zero-shear rate viscosity (Pa s) |
|---|---|
| PS | $8.4 \times 10^4$ |
| PS + 5% clay | $1.0 \times 10^5$ |
| PMMA | $3.2 \times 10^5$ |
| PMMA + 5% clay | $7.9 \times 10^5$ |

the zero-shear rate viscosity. On the other hand, even for nanocomposites, $\eta_0$ is related to material's rheology at very low shear rates when the influence of shear on viscosity is minimal. Hence, the $\eta_0$ values for pure polymers and nanocomposies may be compared. The $\eta_0$ values for PS and PMMA and corresponding Cloisite 6A nanocomposites determined at 170 °C are listed in Table 3. From Figure 10 and Table 3, we can see that at 170 °C the introduction of 5% of Cloisite 6A into the PS matrix results in insignificant (less than 20%) increase in $\eta_0$ from $8.4 \times 10^4$ to $1.0 \times 10^5$ Pa s. On the other hand, the same amount of clay added to PMMA results in an increase of the viscosity from $3.2 \times 10^5$ to $7.9 \times 10^5$ Pa s.

The values of $\eta_0$ are related to the tracer diffusion coefficient through the Einstein relationship according to

$$D = \frac{k_B T}{[\eta_0 k_B / G(M) F(M,\nu)]} \tag{3}$$

where $G(M)$ is a function related to the entanglement molecular weight obtained from the shear modulus of the melt on the rubbery plateau and $F(M,\nu)$ depends on the microstructual parameters of the polymer.[16−18]

If we compare the tracer diffusion coefficients for the filled and unfilled (Figure 1b,d; Table 2) bilayer systems, we find $D/D_0$ (PS) = 1.0(1), which is consistent with the minimal change observed in the bulk viscosity $\eta_{0(\text{unfilled})}/\eta_{0(\text{filled})} = 0.85(9)$. On the other hand for PMMA with the same overall filler concentration, $D/D_0$ (PMMA) = 0.35(3), which is in good agreement with $\eta_{0(\text{unfilled})}/\eta_{0(\text{filled})} = 0.40(4)$ obtained from the bulk measurements.

In the case of bulk measurements it is known that the degree of exfoliation of Cloisite 6A in PS is significantly lower than in PMMA.[19] This is in contrast to the situation in thin films where the degree of exfoliation is high in both cases. Hence the difference in the viscosities and the tracer diffusion coefficients is not simply related to the exfoliation, but is probably due to the difference in the interactions between the polymer matrix and the surface of the clay platelets. The precise nature of the chemical interaction is currently being studied using spectroscopic techniques and will be described elsewhere.

## Conclusions

Scanning force and transmission electron microscopy measurements have shown that spin casting films of functionlized organosilicate clays and polymers produces a high degree of exfoliation in both PS and PMMA matrices. Secondary ion mass spectrometry measurements show that in both cases the platelets are dispersed within the polymer films, but their mobilities are low compared to that of the polymer chains. In the case of PS, addition of 5 vol % clay does not affect the tracer diffusion coefficient, whereas in the case of PMMA the tracer diffusion coefficient is reduced by a factor of 3 with the addition of the same clay volume fraction. Rheological measurements on melt mixed samples of PS or PMMA with the same volume fraction of Cloisite 6A clay indicate that the extrapolated zero shear viscosity is unaffected by the addition of clay in PS and is reduced by a factor of 3 in PMMA. These differences, which are in good agreement with the diffusion measurements, are ascribed to preferential adsorption of the PMMA chains to the surface of the clay platelets which hinder chain mobility.

## References and Notes

(1) Blumstein, A. *J. Polym. Sci., Part A* **1965**, *3*(7PA), 2665 and 2653.
(2) Sherman, L. M. *Plast. Technol.* **1999**, June.
(3) DeGaspari, J. *Mech. Eng.* **2001**, *123* (4), 52.
(4) Okada, A.; Kawasumi, M.; Usuki, A.; Kojima, Y.; Kurauchi, T.; Kamigaito, O. *Mater. Res. Soc. Proc.* **1990**, *171*, 45−50.
(5) Vaia, R. A.; Giannelis, E. P. Polymer Nanocomposites Status and Opportunities. *MRS Bull.* **2001**, May, 394−401.
(6) Krishnamoorti, R.; et al. *Chem. Mater.* **1996**, *8*, 1728−1734.
(7) Krishnamoorti, R.; et al. *Macromolecules* **1997**, *30*, 4097−4102.
(8) Yoon, J. T.; et al. *Polymer* **2001**, *42*, 329−336.
(9) Kim, J.; et al. *J. Appl. Polym. Sci.* **2001**, *80*, 592−603.
(10) Ryu, J.; et al. *Kor.-Austr. Rheol. J.* **2001**, *13* (2), 61−65.
(11) Shin, K.; et al. *MRS Proc.* **2001**, *661*.
(12) Crank, J. *The Mathematics of Diffusion*, 2nd ed., Oxford University Press: Oxford, England, 1975.
(13) Frank, J.; Park, G. S. *Diffusion in Polymers*; Academic Press: San Diego, CA, 1968.
(14) Helleloid, G. T. *J. Appl. Math.* **2001.**
(15) Malkin, A. Y. Rheology of Filled Polymers. *Adv. Polym. Sci.* **1996**, 69−97.
(16) Fox, T. G.; Allen, V. R. *J. Chem. Phys.* **1964**, *41*, 344−352.
(17) Berry, G. C.; Fox, T. G. *Adv. Polym. Sci.* **1968**, *5*, 261.
(18) Green, P. F.; Kramer, E. J. *J. Mater. Res.* **1986**, *1* (1), 202−204.
(19) Si, M.; et al. *APS Meeting* **2002**, Spring.

MA020937F